

MeV bremsstrahlung X rays from intense laser interaction with solid foils

S. Palaniyappan¹, D. C. Gautier¹, B. J. Tobias¹, J. C. Fernandez¹, J. Mendez¹, T. Burris-Mog¹, C. K. Huang¹, A. Favalli¹, J. F. Hunter¹, M. E. Espy¹, D. W. Schmidt¹, R. O. Nelson¹, A. Sefkow², T. Shimada¹ and R. P. Johnson¹

¹Los Alamos National Laboratory, Los Alamos, New Mexico 87545, USA and ²University of Rochester, New York 14627, USA

Research Article

Cite this article: Palaniyappan S *et al.* (2018). MeV bremsstrahlung X rays from intense laser interaction with solid foils. *Laser and Particle Beams* **36**, 502–506. <https://doi.org/10.1017/S0263034618000551>

Received: 16 November 2018

Revised: 5 December 2018

Accepted: 6 December 2018

Key words:

Intense laser–plasma; MeV X-ray radiography

Author for correspondence:

S. Palaniyappan, Los Alamos National Laboratory, Los Alamos, NM-87545, USA,
E-mail: sasi@lanl.gov

Abstract

Laser-based compact MeV X-ray sources are useful for a variety of applications such as radiography and active interrogation of nuclear materials. MeV X rays are typically generated by impinging the intense laser onto ~mm-thick high-Z foil. Here, we have characterized such a MeV X-ray source from 120 TW (80 J, 650 fs) laser interaction with a 1 mm-thick tantalum foil. Our measurements show X-ray temperature of 2.5 MeV, flux of 3×10^{12} photons/sr/shot, beam divergence of ~0.1 sr, conversion efficiency of ~1%, that is, ~1 J of MeV X rays out of 80 J incident laser, and source size of 80 μ m. Our measurement also shows that MeV X-ray yield and temperature is largely insensitive to nanosecond laser contrasts up to 10^{-5} . Also, preliminary measurements of similar MeV X-ray source using a double-foil scheme, where the laser-driven hot electrons from a thin foil undergoing relativistic transparency impinging onto a second high-Z converter foil separated by 50–400 μ m, show MeV X-ray yield more than an order of magnitude lower compared with the single-foil results.

Introduction

Compact MeV X-ray sources are useful for several applications such as radiography and active interrogation of nuclear materials (Courtois *et al.*, 2011). Intense lasers can generate multi-MeV hot electrons when interacting with a ~mm-thick high-Z foils such as tungsten or tantalum. In these targets, the laser couples its energy to the hot electrons mainly on the target surface via several physical processes (Malka and Miquel, 1996; Wilks and Kruer, 1997; Santala *et al.*, 2000). Subsequently, the hot electrons generate MeV bremsstrahlung X rays as they traverse through the rest of the high-Z foil. Several experiments have characterized such intense laser-driven bremsstrahlung X-ray sources (Perry *et al.*, 1999; Edwards *et al.*, 2002; Clarke *et al.*, 2006; Hayashi *et al.*, 2006; Galy *et al.*, 2007; Courtois *et al.*, 2011; Courtois *et al.*, 2013; La Fontaine, 2014; Liang *et al.*, 2016; Chen *et al.*, 2017; Yang *et al.*, 2017).

Here, we have characterized such a MeV bremsstrahlung X-ray source from 120 TW (80 J, 650 fs) Trident laser at the Los Alamos National Laboratory interacting with a 1 mm-thick tantalum foil. Our measurements show X-ray temperature of 2.5 MeV, flux of 3×10^{12} photons/sr/shot, beam divergence of ~0.1 sr, conversion efficiency of ~1%, that is, ~1 J of MeV X rays out of 80 J incident laser, and source size of 80 μ m. Our measurement also shows that MeV X-ray yield and temperature is largely insensitive to nanosecond laser contrast up to 10^{-5} .

In contrast, numerical simulations have shown that a double-foil scheme, where laser-driven hot electrons from a thin foil that undergoes relativistic transparency (Kaw and Dawson, 1970; Palaniyappan *et al.*, 2012, 2015) impinging onto a separate high-Z converter foil, could generate more efficient K_{α} X rays than the single-foil scheme (Sefkow *et al.*, 2011). The same reasoning can also be extended to MeV X-ray generation. Our preliminary measurements of MeV X-ray source using the double-foil scheme, where the laser-driven hot electrons from a thin foil (110 nm aluminum foil) undergoing relativistic transparency (Kaw and Dawson, 1970; Palaniyappan *et al.*, 2012, 2015; Cobble *et al.*, 2016) impinging onto a second high-Z converter foil separated by 50–400 μ m, show MeV X-ray yield more than an order of magnitude lower compared with the single-foil results discussed above. We believe that a better understanding of the hot electron transport in vacuum from the thin foil to the converter foil could help optimize the double-foil scheme. Also, reducing the gap between the two foils down to 20 μ m or lower as indicated in Sefkow *et al.* (2011) could also help mitigate the hot electron transport issues. Although understanding and optimizing the double-foil scheme could potentially yield a better MeV bremsstrahlung X-ray source, it is beyond the scope of the present work.

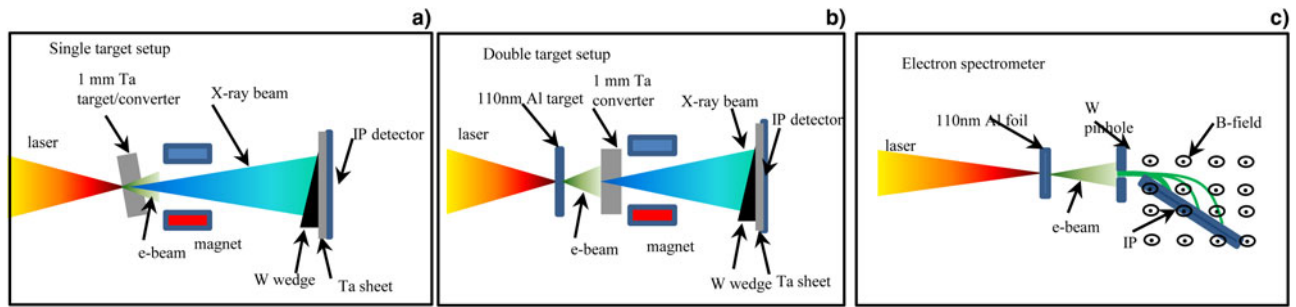


Fig. 1. Schematic representation of experimental setup ($f/3$ laser focus onto 110 nm Al foil). (a) The 0.12 PW Trident laser is focused with $f/3$ off-axis-parabola (peak intensity $\sim 2 \times 10^{20}$ W/cm²) onto a 1 mm-thick tantalum foil (foil normal rotated 10° off to laser propagation axis). The tantalum foil acts both as electron source and X-ray converter. A 0.2 T magnet deflects the charged particles away. The X-ray transmission through the tungsten wedge (5.08 cm \times 5.08 cm \times 17.8 cm) is measured using a calibrated BAS-SR Fuji image plate (20 cm \times 40 cm). The image plate was covered with a 0.5 mm-thick tantalum sheet (20 cm \times 40 cm) to block X rays below 92 keV ($<1\%$ transmission at 92 keV) reaching the image plate detector. The X-ray spectrum is retrieved from the transmission data via Expectation-Maximization algorithm. (b) Double-foil scheme: same setup as before except the laser impinges onto a 110 nm-thick aluminum foil. The electron beam from the aluminum foil subsequently impinges onto a 1 mm-thick tantalum X-ray converter foil. The spacing between the foils was varied from 50 to 400 μ m. (c) Schematic representation of the magnetic electron spectrometer used to measure the electron spectrum from 110 nm Al foil. A 1 mm diameter tungsten pinhole was placed 15 cm away from the converter foil to sample the electron beam.

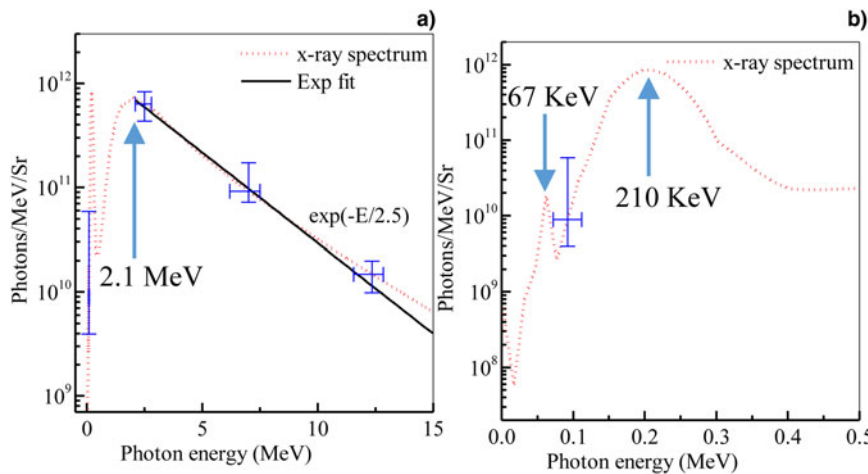


Fig. 2. Results from single target setup. (a) Measured X-ray spectrum from single 1 mm-thick tantalum foil. (b) Closer view of the same X-ray spectrum showing spectral peaks at 67 and 210 keV.

Experimental setup

The experiments reported here were conducted at the Trident laser facility at the Los Alamos National Laboratory, USA (Batha *et al.*, 2008). The Trident laser (80 J, 650 fs FWHM, 1053 nm wavelength, *s*-polarization) is focused onto the target using an $f/3$ off-axis parabola to a spot size of 10 μ m diameter (first Airy minimum containing 65% laser energy) with a peak laser intensity of 2×10^{20} W/cm² ($a_0 \approx 13$). Plasma mirrors were not used in the experiment.

The laser is incident on a 1 mm-thick tantalum foil that is rotated 10° off the laser axis (see Fig. 1a). A 0.2 T magnet, 5.5 cm long, located right behind the tantalum foil deflected the charged particles away from reaching the X-ray detector. The X-ray transmission through a tungsten wedge, thickness ranging from 0 to 5.08 cm over a length of 17.8 cm, was measured using a calibrated image plate detector (Fernandez *et al.*, 2017). An additional 0.5 mm-thick tantalum foil covered the entire image plate to block X rays below 92 keV ($<1\%$ transmission at 92 keV).

For the double-foil scheme, shown in Figure 1(b), the intense laser, incident normally on a 110 nm-thick aluminum foil that undergoes relativistic transparency, drives a multi-MeV electron

beam. These hot electrons impinge onto a 1 mm-thick tantalum foil that is 50–200 μ m away from the aluminum foil. The electron beam generates bremsstrahlung MeV X rays as they traverse through the high-Z converter foil. These X rays are measured the same way as discussed above.

We also used a separate magnetic spectrometer, 0.8 T magnetic field over 10 cm long, to measure the electron spectrum from the aluminum foil (Fig. 1c). The tungsten pinhole (1 mm diameter) was placed 15 cm away from the converter foil. The image plate detector (BAS-TR) was placed inside the magnet opening at 33.7° angle with respect to the incident electron trajectory to capture the deflected electrons. The lower (higher) energy cut-off of the magnetic spectrometer was 0.2 MeV (28.2 MeV).

Results and Discussion

Figure 2(a) shows the X-ray spectrum retrieved from the measured X-ray transmission data when the Trident laser is incident on a 1 mm-thick tantalum foil. The X-ray spectrum peaks at 2.1 MeV with a temperature of 2.5 MeV. The X-ray spectral peak at 210 keV appears from the tantalum filter. Additionally, the X-ray spectrum shows a tantalum *K*-edge at 67 keV

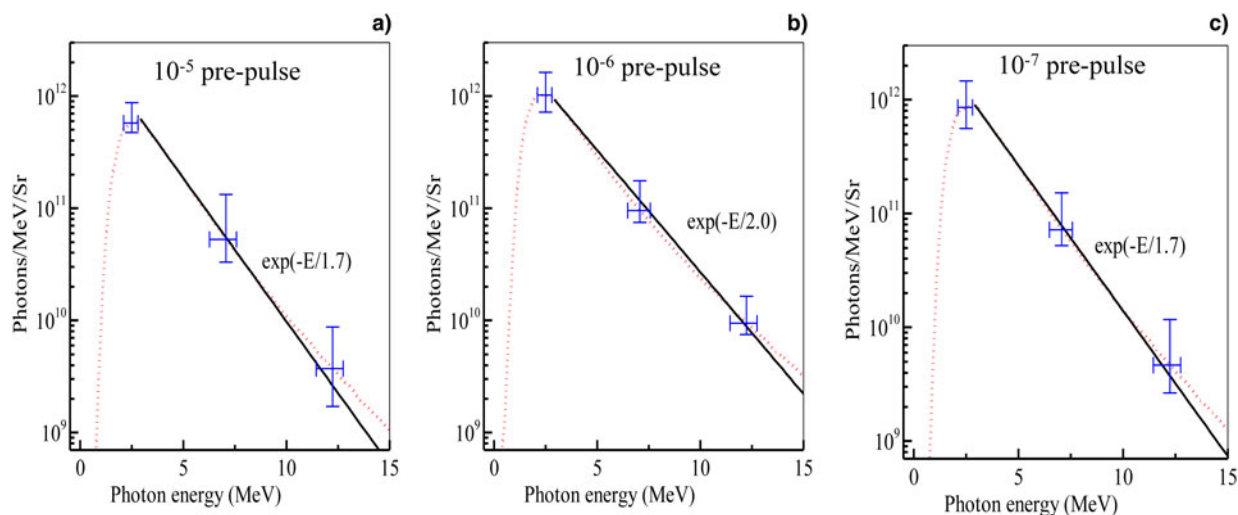


Fig. 3. Effect of laser contrast on X-ray spectrum from single 1 mm-thick tantalum foil. A 1 ns-long pedestal at various laser intensity levels were added to the high-contrast Trident laser. Measured X-ray spectra when added (a) 10^{-5} pedestal, (b) 10^{-6} pedestal, and (c) 10^{-7} pedestal.

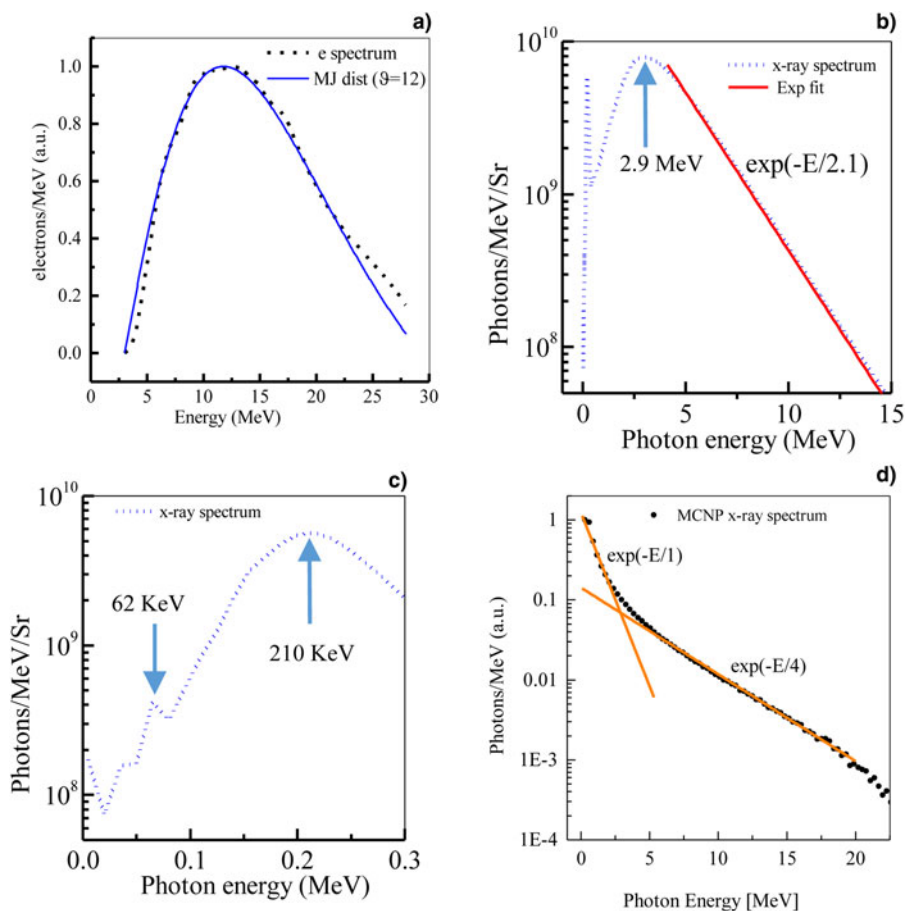


Fig. 4. Results from double target setup. (a) Measured electron spectrum from 100 nm-thick aluminum foil using a magnetic spectrometer. (b) Measured X-ray spectrum from double target (100 nm-thick aluminum foil $\sim 200 \mu\text{m}$ away from 1 mm-thick tantalum converter foil). (c) Zoomed in view of the same X-ray spectrum showing spectral peaks at 67 and 210 keV. (d) Simulated X-ray spectrum using measured electron spectrum as input to Monte-Carlo algorithm MCNP.

(Fig. 2b). However, the 67 and 210 keV X-ray peaks have negligible X-ray energy content compared with the broader 2.1 MeV peak. The integrated X-ray spectrum yields 2.5×10^{12} photons/sr per shot. The yield varied typically by less than a factor of two from shot-to-shot. For the X-ray beam FWHM divergence of 0.1 sr (10° half-opening angle), we get 0.8 J of MeV X rays, which is $\sim 1\%$ conversion efficiency.

Additionally, we also tested the sensitivity of the X-ray generation from the single-foil target to the ns pre-pulse/pedestal. We added 1 ns long pre-pulses that were at the 10^{-5} (Fig. 3a), 10^{-6} (Fig. 3b), and 10^{-7} (Fig. 3c) level compared with the peak of the high-contrast high-power Trident laser pulse. The measured X-ray spectrum shows that the added pre-pulses do not have a significant effect on the X-ray spectra and the yield from the

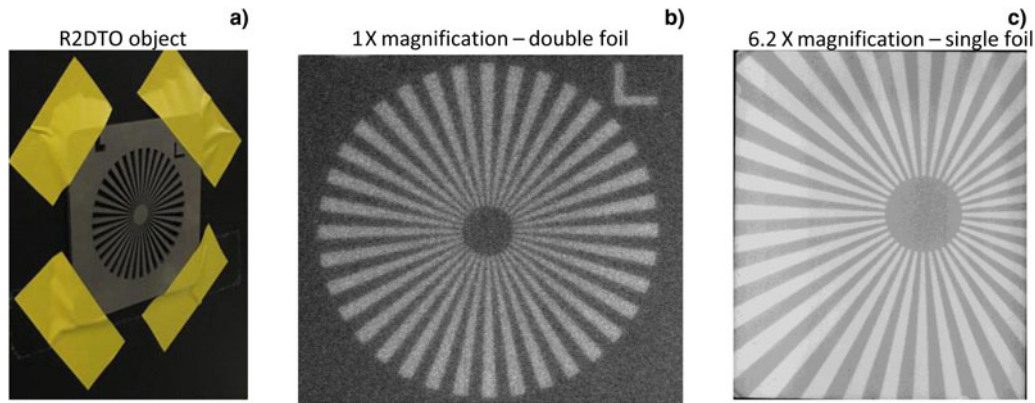


Fig. 5. MeV X-ray radiograph. (a) 10 cm × 10 cm × 6 mm tungsten object called “R2DTO” with radial slots used for measuring the MeV X-ray source size, (b) radiograph of R2DTO taken using MeV X rays from the double-foil scheme with 1:1 magnification, (c) radiograph of the same object using MeV X rays from the single-foil scheme with 6.2 × magnification.

1 mm-thick tantalum foil. For this setup, we added an extra 4 mm-thick tungsten filter to block X rays below 240 keV (<1% transmission below 240 keV). Hence, the 67 and 210 keV X-ray peaks are missing in Figure 3a–c. One-dimensional HELIOS radhydro (MacFarlane *et al.*, 2006) simulation showed that these prepulses produce a pre-plasma density gradient of only a few microns at the front surface of the target due to lower sound speed of the heavier ions. Also here we use *s*-polarized laser where the laser *E*-field has no component along the pre-plasma gradient that could reduce the vacuum heating in the pre-plasma (Brunel, 1987).

Figure 4a shows the electron spectrum (dashed red line) from the 110 nm aluminum foil measured using the magnetic spectrometer. The electron spectrum peaks around 12 MeV. The instrument had a lower (higher) energy cut-off of 0.2 (28.2) MeV. It is possible that the low-energy electrons below 3 MeV do not escape the target (Cobble *et al.*, 2016). The measured electron spectrum matches well with a Maxwell–Jüttner distribution $f(E) = (E^2\beta/\theta K_2(1/\theta))\exp(-E/\theta)$ with $\theta = kT/mc^2 = 12$, where $\beta = v/c$, and kT is the electron temperature. Figure 4b shows the typical X-ray spectrum retrieved from the measured X-ray transmission data from the double-foil targets with ~200 μm spacing between them via Expectation-Maximization algorithm (Lange and Carson, 1984; Zhang *et al.*, 2007). Varying the distance between foils from 50 to 400 μm did not seem to affect the X-ray spectra and yield in any consistent manner. The X-ray spectrum peaks at 210 keV and 2.9 MeV with a temperature of 2.1 MeV. Additionally, the X-ray spectrum shows a tantalum k_α peak at 67 keV (Fig. 4c). However, the 67 and 210 keV X-ray peaks have negligible X-ray energy content compared with the broader 2.9 MeV peak. It is most likely that the 210 keV X-ray peak is an apparent peak due to significant X-ray filtering from the 0.5 mm-thick tantalum foil.


Figure 4d shows the simulation results when an electron beam with the measured electron spectrum in Figure 4a traverses through a 1 mm-thick tantalum converter foil using the code Monte Carlo N-Particle (MCNP) (Forster and Godfrey, 1985). The simulation results show a two temperature (1 and 4 MeV) X-ray spectrum that has no obvious spectral peaks. The fact that the X-ray spectrum from the MCNPX simulation (Fig. 4d) is much hotter than the measured X-ray distribution (Fig. 4b) seems to provide evidence that there may be issues in the transport of the hot electrons from the thin foil to the converter foil.

We believe that better understanding of the hot electron transport from the thin foil to the converter foil could help optimize the double-foil scheme. Also, reducing the gap between the two foils down to 20 μm or lower as indicated in Sefkow *et al.* (2011) could help mitigate the hot electron transport issues. The integrated X-ray spectrum from the double-foil scheme yields 3.6×10^{10} photons/sr per shot. However, the yield varied by more than one order of magnitude from shot-to-shot.

Figure 5a shows the R2DTO object, a 10 cm × 10 cm × 6 mm tungsten object with radial slots, used for quantifying the MeV X-ray source size from the X-ray radiograph of the object using the Bayesian-Inference-Engine (BIE) analysis. Figure 5b shows R2DTO radiograph using the X rays from the double-foil source with 1:1 magnification. Figure 5c shows the same radiograph using the X rays from the single-foil source with 6.2 × magnification. The images show that the edges of the radial slots are blurred when using the double-foil X-ray source. The BIE analysis of these images shows that the MeV X-ray source size was 35–195 and 270–600 μm in the single-foil and double-foil schemes, respectively. The details of the BIE analysis is discussed elsewhere (Tobias *et al.*, 2017). The larger source size in the double-foil scheme could come from the hot electron transport issues that could increase the size of the electron beam reaching the converter foil.

Conclusions

In conclusion, we have characterized MeV bremsstrahlung X-ray source from 120 TW (80 J, 650 fs) Trident laser interaction with a 1 mm-thick tantalum foil. Our measurements show X-ray temperature of 2.5 MeV, flux of 3×10^{12} photons/sr/shot, beam divergence of ~0.1 sr, conversion efficiency of ~1%, that is, ~1 J of MeV X rays out of 80 J incident laser, and source size of 80 μm. Our measurement also shows that MeV X-ray yield and temperature is largely insensitive to nanosecond laser contrast up to 10^{-5} . Also, preliminary measurements of similar MeV X-ray source using a double-foil scheme, where the laser-driven hot electrons from a thin foil undergoing relativistic transparency impinging onto a second high-Z converter foil separated by 50–400 μm, show MeV X-ray yield more than an order of magnitude lower compared with the single-foil results. Despite the interest, further optimization and complete understanding of the double-foil scheme using comprehensive Particle-In-Cell (PIC) simulations is beyond the scope of the work presented here.

Author ORCID.  S. Palaniyappan 0000-0001-6377-1206.

Acknowledgments. This work was performed under the auspices of the National Nuclear Security Administration Inertial Confinement Fusion Program John Kline, LANL ICF Program Manager along with the support of the Los Alamos National Laboratory LDRD (Laboratory Directed Research and Development) project 20170573ECR. This work was funded in part by DOE-NNSA.

References

- Batha SH, Aragonez R, Archuleta FL, Archuleta TN, Benage JF, Cobble JA, Cowan JS, Fatherley VE, Flippo KA, Gautier DC, Gonzales RP, Greenfield SR, Hegelich BM, Hurry TR, Johnson RP, Kline JL, Letzring SA, Loomis EN, Lopez FE, Luo SN, Montgomery DS, Oertel JA, Paisley DL, Reid SM, Sanchez PG, Seifter A, Shimada T and Workman JB (2008) TRIDENT high-energy-density facility experimental capabilities and diagnostics. *Review of Scientific Instruments* **79** (10), 10F305-1–10F305-3.
- Brunel F (1987) Not-so-resonant, resonant absorption. *Physical Review Letters* **59**(1), 52–55.
- Chen H, Hermann MR, Kalantar DH, Martinez DA, Di Nicola P, Tommasini R, Landen OL, Alessi D, Bowers M, Browning D, Brunton G, Budge T, Crane J, Di Nicola JM, Doppner T, Dixit S, Erbert G, Fishler B, Halpin J, Hamamoto M, Heebner J, Hernandez VJ, Hohenberger M, Homoelle D, Honig J, Hsing W, Izumi N, Khan S, LaFortune K, Lawson J, Nagel SR, Negres RA, Novikova L, Orth C, Pelz L, Prantil M, Rushford MM, Shaw M, Sherlock M, Sigurdsson R, Wegner P, Widmayer C, Williams GJ, Williams W, Whitman P and Yang S (2017) High-energy (>70 keV) x-ray conversion efficiency measurement on the ARC laser at the National Ignition Facility. *Physics of Plasmas* **24**(3), 033112-1–033112-9.
- Clarke RJ, Neely D, Edwards RD, Wright PNM, Ledingham KWD, Heathcote R, McKenna P, Danson CN, Brummitt PA, Collier JL, Hatton PE, Hawkes SJ, Hernandez-Gomez C, Holligan P, Hutchinson MHR, Kidd AK, Lester WJ, Neville DR, Norreys PA, Pepler DA, Winstone TB, Wyatt RWW and Wyborn BE (2006) Radiological characterisation of photon radiation from ultra-high-intensity laser-plasma and nuclear interactions. *Journal of Radiological Protection* **26** (3), 277–286.
- Cobble JA, Palaniyappan S, Johnson RP, Shimada T, Huang C, Gautier DC, Clark DD, Falk K and Jung D (2016) Laser-driven micro-Coulomb charge movement and energy conversion to relativistic electrons. *Physics of Plasmas* **23**(9), 093113-1–093113-12.
- Courtois C, Edwards R, La Fontaine AC, Aedy C, Barbotin M, Bazzoli S, Biddle L, Brebion D, Bourgade JL, Drew D, Fox M, Gardner M, Gazave J, Lagrange JM, Landoas O, Le Dain L, Lefebvre E, Mastro Simone D, Pichoff N, Pien G, Ramsay M, Simons A, Sircombe N, Stoeckl C and Thorp K (2011) High-resolution multi-MeV x-ray radiography using relativistic laser-solid interaction. *Physics of Plasmas* **18**(2), 023101-1–023101-5.
- Courtois C, Edwards R, La Fontaine AC, Aedy C, Bazzoli S, Bourgade JL, Gazave J, Lagrange JM, Landoas O, Le Dain L, Mastro Simone D, Pichoff N, Pien G and Stoeckl C (2013) Characterisation of a MeV Bremsstrahlung x-ray source produced from a high intensity laser for high areal density object radiography. *Physics of Plasmas* **20**(8), 083114-1–083114-8.
- Edwards RD, Sinclair MA, Goldsack TJ, Krushelnick K, Beg FN, Clark EL, Dangor AE, Najmudin Z, Tatarakis M, Walton B, Zepf M, Ledingham KWD, Spencer I, Norreys PA, Clarke RJ, Kodama R, Toyama Y and Tampo M (2002). Characterization of a gamma-ray source based on a laser-plasma accelerator with applications to radiography. *Applied Physics Letters* **80**(12), 2129–2131.
- Fernandez JC, Gautier DC, Huang CK, Palaniyappan S, Albright BJ, Bang W, Dyer G, Favalli A, Hunter JF, Mendez J, Roth M, Swinhoe M, Bradley PA, Deppert O, Espy M, Falk K, Guler N, Hamilton C, Hegelich BM, Henzlova D, Ianakiev KD, Iliev M, Johnson RP, Kleinschmidt A, Losko AS, McCary E, Mocko M, Nelson RO, Roycroft R, Cordoba MAS, Schanz VA, Schaumann G, Schmidt DW, Sefkow A, Shimada T, Taddeucci TN, Tebartz A, Vogel SC, Vold E, Wurden GA and Yin L (2017) Laser-plasmas in the relativistic-transparency regime: science and applications. *Physics of Plasmas* **24**(5), 056702-1–056702-19.
- Forster RA and Godfrey TNK (1985) Mcnp – a general Monte-Carlo code for neutron and photon transport. *Lecture Notes in Physics* **240**, 33–55.
- Galy J, Maucec M, Hamilton DJ, Edwards R and Magill J (2007) Bremsstrahlung production with high-intensity laser matter interactions and applications. *New Journal of Physics* **9**, 23-1–23-18.
- Hayashi Y, Fukumi A, Matsukado K, Mori M, Kotaki H, Kando M, Chen LM, Daito I, Kondo S, Kanazawa S, Yamazaki A, Ogura K, Nishiuchi M, Kado M, Sagisaka A, Nakamura S, Li Z, Orimo S, Homma T and Daido H (2006) Estimation of photon dose generated by a short pulse high power laser. *Radiation Protection Dosimetry* **121**(2), 99–107.
- Kaw P and Dawson J (1970) Relativistic nonlinear propagation of laser beams in cold over dense plasmas. *Physics of Fluids* **13**, 472–8.
- La Fontaine AC (2014) Photon dose produced by a high-intensity laser on a solid target. *Journal of Physics D-Applied Physics* **47**(32), 325201-1–325201-18.
- Lange K and Carson R (1984) Em reconstruction algorithms for emission and transmission tomography. *Journal of Computer Assisted Tomography* **8**(2), 306–316.
- Liang T, Bauer J, Cimeno M, Ferrari A, Galtier E, Granados E, Lee HJ, Liu J, Nagler B, Prinz A, Rokni S, Tran H and Woods M (2016) Radiation dose measurements for high-intensity laser interactions with solid targets at slac. *Radiation Protection Dosimetry* **172**, 346–355.
- MacFarlane JJ, Golovkin IE and Woodruff PR (2006) HELIOS-CR – a 1-D radiation-magnetohydrodynamics code with inline atomic kinetics modeling. *Journal of Quantitative Spectroscopy & Radiative Transfer* **99**(1–3), 381–397.
- Malka G and Miquel JL (1996) Experimental confirmation of ponderomotive-force electrons produced by an ultrarelativistic laser pulse on a solid target. *Physical Review Letters* **77**(1), 75–78.
- Palaniyappan S, Hegelich BM, Wu HC, Jung D, Gautier DC, Yin L, Albright BJ, Johnson RP, Shimada T, Letzring S, Offermann DT, Ren J, Huang CK, Horlein R, Dromey B, Fernandez JC and Shah RC (2012) Dynamics of relativistic transparency and optical shuttering in expanding overdense plasmas. *Nature Physics* **8**(10), 763–769.
- Palaniyappan S, Huang CK, Gautier DC, Hamilton CE, Santiago MA, Kreuzer C, Sefkow AB, Shah RC and Fernandez JC (2015) Efficient quasi-monoenergetic ion beams from laser-driven relativistic plasmas. *Nature Communications* **6**, 10170-1–10170-12.
- Perry MD, Sefcik JA, Cowan T, Hatchett S, Hunt A, Moran M, Pennington D, Snavely R and Wilks SC (1999) Hard x-ray production from high intensity laser solid interactions (invited). *Review of Scientific Instruments* **70**(1), 265–269.
- Santala MIK, Zepf M, Watts I, Beg FN, Clark E, Tatarakis M, Krushelnick K, Dangor AE, McCanny T, Spencer I, Singhal RP, Ledingham KWD, Wilks SC, Machacek AC, Wark JS, Allott R, Clarke RJ and Norreys PA (2000) Effect of the plasma density scale length on the direction of fast electrons in relativistic laser-solid interactions. *Physical Review Letters* **84**(7), 1459–1462.
- Sefkow AB, Bennett GR, Geissel M, Schollmeier M, Franke BC and Atherton BW (2011) Efficiency enhancement for K-alpha x-ray yields from laser-driven relativistic electrons in solids. *Physical Review Letters* **106**(23), 255002-1–255002-4.
- Tobias BT, Palaniyappan S, Gautier DC, Mendez J, Burris-Mog T, Huang CK, Favalli A, Hunter JF, Espy ME, Schmidt DW, Nelson RO, Sefkow A, Shimada T, Johnson RP and Fernandez JC (2017) Quantification of uncertainty in photon source spot size inference during laser-driven radiography experiments at TRIDENT. LA-UR-17-28604.
- Wilks SC and Kruer WL (1997) Absorption of ultrashort, ultra-intense laser light by solids and overdense plasmas. *IEEE Journal of Quantum Electronics* **33**(11), 1954–1968.
- Yang B, Qiu R, Li JL, Lu W, Wu Z and Li CY (2017) Photon dose estimation from ultraintense laser-solid interactions and shielding calculation with Monte Carlo simulation. *Radiation Physics and Chemistry* **131**, 13–21.
- Zhang L, Zhang GW, Chen ZQ, Xing YX, Cheng JP and Xiao YS (2007) X-ray spectrum estimation from transmission measurements using the expectation maximization method. 2007 IEEE Nuclear Science Symposium Conference Record, Vols 1-11: 3089-3093.